MENU 2007
11th International Conference
on Meson-Nucleon Physics and
the Structure of the Nucleon
September 10-14, 2007
IKP, Forschungzentrum Jülich, Germany

# THREE-BODY FORCE EFFECTS IN NEUTRON-DEUTERON SCATTERING AT 95 MeV

*J. Blomgren, P. Mermod, C. Johansson, J. Klug, L. Nilsson, N. Olsson*[1], *S. Pomp, U. Tippawan*[2], *A. Öhrn, M. Österlund*
Department of Neutron Research
Uppsala University
Uppsala, Sweden

*B. Bergenwall, P. Nadel-Turonski*[3]
Department of Radiation Sciences
Uppsala University
Uppsala, Sweden

*O. Jonsson, A. Prokofiev, P.-U. Renberg*
The Svedberg Laboratory
Uppsala University
Uppsala, Sweden

*Y. Maeda, H. Sakai, A. Tamii*
Department of Physics
Tokyo University
Tokyo, Japan

**Abstract**

Three-body force effects have been studied in neutron-deuteron scattering at 95 MeV. Three different experiments, performed with different experimental setups, have been used to provide data covering the full angular distribution with unprecedented precision in the region of the cross section minimum, where three-nucleon forces are expected to be significant. The use of different

[1]Also at Swedish Defence Research Agency, Stockholm, Sweden
[2]Also at Fast Neutron Research Facility, Chiang Mai University, Chiang Mai, Thailand
[3]Presently at George Washington University, Washington, D.C., USA

setups allow detailed studies of systematic effects in the experimental data. Measurements of the ratio between neutron-proton and neutron-deuteron scattering have been performed to provide data free from systematic uncertainties related to cross-section normalization. The data display significant deviations from predictions based on two-nucleon interactions only, while they are perfectly described by theories including three-nucleon forces.

# 1 Introduction

The nucleon-nucleon ($NN$) interaction can be used as a basic tool to describe the properties and interactions of nuclei. For this purpose, $NN$ potentials, which are based on meson-exchange theories, have been developed: the most widely used ones are the Paris potential [1], the Argonne AV18 potential [2], the CD-Bonn potential [3, 4] and the Nijmegen potentials [5]. After proper adjustment of the free parameters, these models are able to describe very well a restricted *pp* and *np* data base below 350 MeV [6].

The next step to demonstrate the success of this approach is to test the $NN$ potentials in three-nucleon ($3N$) systems. Quantitative descriptions of $3N$ systems can be provided rigorously by using $NN$ potentials in the Faddeev equations [7]. However, theoretical considerations indicate that the description of systems made of more than two nucleons is not complete if three-body forces are not taken into account (and, in principle, also four-body forces, five-body forces, etc.). Formally, $3N$ forces can be represented by introducing a $3N$ potential in the Faddeev equations. The most widely used $3N$ potentials are the Tucson-Melbourne [8,9] and Urbana [10,11] forces. As a first experimental evidence, the $^3$H and $^3$He binding energies can be reproduced model-independently taking $3N$ forces into account [12], while calculations using only $NN$ interactions underestimate them by typically half an MeV [3]. Interestingly, the $^4$He binding energy can also be described correctly with combined $NN$ and $3N$ forces [13], indicating that the role of four-nucleon forces is not significant.

The ultimate goal of nuclear physics would be to have a single consistent theory that could describe both nucleon and nuclear properties and dynamics. As pointed out in, e.g., Refs. [6] and [14], an appropriately tailored effective field theory, rooted in the symmetries of QCD, might be a tool powerful enough to succeed in such an ambitious program, at least for few-nucleon systems. In particular, chiral symmetry breaking can be analyzed in terms of an effective field theory, called chiral perturbation theory (CHPT). This model can be applied to describe consistently the interaction between pions and nucleons, as well as the pion-pion interaction. Calculations made within

the CHPT framework at next-to-next-to-leading order implicitly include $3N$ forces [15, 16]. Calculations at the next higher order were made recently [17, 18], allowing for instance an excellent description of $NN$ phase shifts.

Experimental investigations of three-nucleon systems are essential for determining the properties of $3N$ forces. Besides the $^3$H and $^3$He binding energies, a number of observables that may reveal the effects of $3N$ forces have been identified. We will concentrate our discussion to nucleon-deuteron scattering in the energy range $65-250$ MeV. At these energies, significant $3N$-force contributions can potentially be seen in the elastic scattering angular distribution [19, 20] as well as for various spin-transfer observables in elastic scattering [7]. In addition, observables in the break-up process in various kinematical configurations are also expected to provide signatures of $3N$ forces [21, 22]. Existing proton-deuteron elastic scattering data between 65 and 250 MeV can be found in Refs. [23–35], and proton-deuteron break-up data in Refs. [36–40]. Except for Refs. [23, 26], these data were obtained with polarized beams, and polarization observables could be extracted. Comparison of experimental analysing powers with theoretical predictions show a puzzling picture where data and predictions agree only partially with each other. Many of these results call for a better understanding of the spin structure of the three-nucleon forces: possible solutions could be a refinement of the $3N$ force terms in CHPT [15] or the introduction of new types of diagrams in the $3N$ potentials [41]. While polarization observables are extremely valuable especially for studying the details of the $3N$ interactions, in order to validate the whole approach of introducing $3N$ forces at all, an observable that would give a clear and unambiguous signal is desirable. As pointed out in, e.g., Ref. [19], the differential cross section of nucleon-deuteron elastic scattering is expected to reveal substantial effects of $3N$ forces in the minimum region of the angular distribution. This can be understood in the following way: the contributions from $NN$ interactions are strongly forward and backward peaked, while the contributions from $3N$ interactions should be roughly isotropic. Thus, the $3N$-force contribution to the cross section would be particularly significant relative to $NN$ interactions in the angular range of the cross-section minimum. Around 100 MeV, the effect of $3N$ forces is expected to increase the cross section by about 30% in the minimum, as predicted [19] by Faddeev calculations including the Tucson-Melbourne $3N$ force [8] with parameters adjusted to the triton binding energy.

Thus, both neutron-deuteron ($nd$) and proton-deuteron ($pd$) elastic scattering differential cross sections should provide robust investigations of $3N$ forces. The existing $pd$ elastic scattering data [23–29, 32–34] tend to show the expected effects in the cross-section minimum: the descriptions are generally improved when taking $3N$ forces into account. The contribution from the

Coulomb interaction in *pd* scattering is not known with certainty to be negligible in the minimum region, thus complicating the interpretation of these results. Recent calculations suggest that Coulomb interactions should not result in significant effects in the minimum of the *pd* elastic scattering angular distribution above 65 MeV [42,43]. The question of Coulomb effects−and thus also the question of $3N$ force effects−can be definitively settled by *nd* scattering experiments. There are *nd* data at 67 MeV [44] consisting essentially of an analyzing power measurement. Three *nd* experiments at 95 MeV, previously reported in Refs. [45–47], agree well with the predictions including $3N$ forces. Existing data at 152 MeV [48] give the same picture. Recent data at 250 MeV [49], together with *pd* data at the same energy [33], reveal an effect in the cross-section minimum which is too large to be accounted for by any theory. At such large energies, part of the explanation for this failure could be the lack of a full relativistic treatment in the calculations. Pioneering studies [50, 51] show that relativistic effects are expected to increase the cross section in the region of backward angles at large energies. At 95 MeV, the energy of the present work, such effects are not expected to contribute significantly.

In the present work, data from three *nd* scattering experiments are presented. By detecting either the scattered neutron or the recoil deuteron, we were able to cover the angular range from 15 to 160 degrees in the c.m. system. By using two different detector setups in various configurations, we could keep the systematic uncertainties under control. Additionally, by measuring the neutron-proton (*np*) scattering differential cross section and, in the case where scattered neutrons were detected, also elastic scattering in carbon (i.e., the $^{12}$C(n,n) reaction), the systematic error due to uncertainties in the normalization factors was minimized.

The present *np* data give supplementary information about the *np* angular distribution at 95 MeV (for previous data, see, e.g., Refs. [52, 53]). In many experiments, neutron cross sections are measured relative to the *np* cross section [53], i.e., it is used as a cross-section standard. Neutron-proton scattering plays an important role in nuclear physics, since it can be used to validate *NN* potentials and to derive a value of the absolute strength of the strong interaction. The extensive database of *np* differential cross sections is not always consistent and, not unrelated, there are still problems with the determination of a precise value of the $\pi NN$ coupling constant [6, 54, 55].

In the *nd* experiment where the scattered neutrons were detected, we could also obtain elastic scattering angular distributions for carbon and oxygen at 95 MeV, which are not discussed further here. Besides their interest in fundamental nuclear theory, these data are relevant for medical treatment of tumors with fast neutrons as well as in dosimetry, since the human body

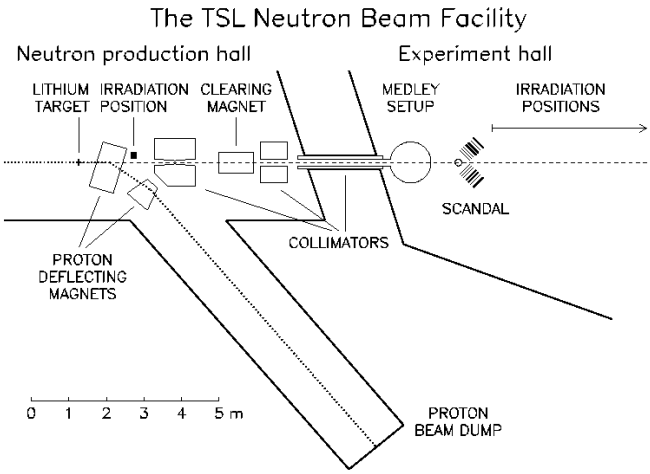


Figure 1: Schematic view of the Uppsala neutron beam facility before its upgrade in 2004.

contains significant amounts of carbon and oxygen. Recoil nuclei from elastic and inelastic scattering are expected to account for more than 10% of the cell damage, the rest being mainly due to *np* scattering and neutron-induced emission of light ions [57, 58]. The oxygen data may also be relevant for future incineration of nuclear waste in subcritical reactors fed by a proton accelerator, where the nuclear fuel might be in oxide form. These data were obtained as by-products of the target handling, e.g., due to the use of heavy water as deuterium target.

# 2 Experimental procedure

## 2.1 Neutron beam and detector setups

A full account of the experimental details and analysis procedures have been published in Ref. [47], and only an introduction is presented here. The present experiments were performed with the two experimental setups MEDLEY [59] and SCANDAL [60] at the neutron beam facility (before upgrade, see Fig. 1) at The Svedberg Laboratory in Uppsala, Sweden. This facility has been described in detail in Ref. [60], and therefore only a brief outline will be given here. The neutrons were produced with the $^7$Li(p,n)$^7$Be reaction, using a 98

MeV proton beam of about 5 $\mu$A hitting an 8 mm thick neutron production target consisting of lithium enriched to 99.98% in $^7$Li. The resulting neutron spectrum consisted of a high-energy peak at 94.8±0.5 MeV with an energy spread of 2.7 MeV (FWHM) and a low-energy tail which was suppressed by time-of-flight techniques. After the production target, the proton beam was bent into a well-shielded beam dump where the beam current was integrated in a Faraday cup for relative beam monitoring consistency checks. At the MEDLEY target position 9.15 m after the neutron production target, the neutron beam was about 8 cm in diameter and had an intensity of about $5\times10^4$ s$^{-1}$cm$^{-2}$. At the SCANDAL target position 10.70 m after the lithium target, the beam was about 9 cm in diameter and had an intensity of about $4\times10^4$ s$^{-1}$cm$^{-2}$. The neutron beam was transported in a vacuum system which was terminated with a 0.1 mm thick stainless steel foil at the exit of the MEDLEY chamber. Immediately after the foil, two fission detectors were mounted for relative monitoring of the neutron fluence: one monitor was based on thin-film breakdown counters (TFBC) [61] and the other one, which was more stable and had much better statistics, on an ionization chamber (ICM). The MEDLEY target, the vacuum chamber exit foil, and the neutron monitors were thin enough to consider the neutron beam as negligibly affected.

The MEDLEY vacuum chamber is a cylinder of 80 cm inner diameter. Targets were mounted onto frames attached to the center of the ceiling, with a remote control allowing to switch between up to three different frames without opening the vacuum chamber. Eight telescopes were placed on rails emerging radially at 20° separation from each other on a rotatable table. Two silicon detectors and one CsI detector could be mounted inside each telescope. Thin (50 or 60 $\mu$m thickness) and thick (400 or 500 $\mu$m thickness) silicon detectors were available. The CsI crystals were thick enough to detect protons with energies up to 110 MeV. This combination of silicon detectors and CsI crystals allowed light ion detection, identification and energy measurement in the energy range 3−110 MeV. In order to define precisely the active detection area (and solid angle), either active plastic scintillators or passive aluminum rings were used as collimators. A full description of the MEDLEY setup is given in Ref. [59].

The SCANDAL (SCAttered Nucleon Detection AssembLy) setup, previously described in Ref. [60], consists of two identical arms that can be positioned on either side of the beam and rotated around the target position. Each SCANDAL arm was equipped with a 2 mm thick veto scintillator for charged-particle rejection, two converter scintillators of 20 mm and 10 mm thickness for neutron-proton conversion, a 2 mm thick $\Delta E$ plastic scintillator for triggering, two drift chambers (DCH) giving two horizontal and

two vertical coordinates for proton tracking, another 2 mm thick $\Delta E$ plastic scintillator for triggering, and an array of twelve CsI detectors that defined twelve angular bins. The CsI detectors as well as the plastic scintillators were read out by photomultiplier (PM) tubes. The CsIs had one PM tube each, and the scintillators two each, mounted adjacent to each other on one of the longer, horizontal sides. The proton energy resolution was on average 3.7 MeV (FWHM) [60], varying between the individual CsI crystals due to internal properties of the detectors. The setup could be used for direct detection of protons or deuterons coming from the target by simply removing the veto and converter scintillators. This option allowed to measure *np* and *nd* elastic scattering at backward angles. In proton/deuteron detection mode, a multitarget (MTGT) box permitted to use up to seven targets at the same time, sandwiched between multiwire proportional counters (MWPCs). In this way it was possible to determine in which target the reaction took place and to veto charged particles in the beam.

# 3 Results and discussion

The final results for *np* and *nd* scattering, recently reported in Refs. [45–47], are shown in Fig. 2. The *nd* differential cross section is shown in the middle panel. For the data in proton/deuteron detection mode, the ratio of *nd* to *np*− a quantity which is independent of the absolute normalization−is plotted in the bottom panel as a function of the proton/deuteron angle in the laboratory.

The *np* data are valuable in the sense that they increase the database in the intermediate energy region, where the systematic uncertainties are not always under satisfying control. Many applications involve measurements relative to the *np* cross section, and new data are therefore most welcome. The *np* data from the three present experiments are in good overall agreement with each other and with predictions based on modern *NN* interactions. This allows us to validate the quality of the *nd* data since the *np* and *nd* differential cross sections were measured under essentially the same conditions.

The *nd* data agree well with each other in the regions where they overlap. We can compare them with Faddeev calculations using various *NN* potentials, and see if the description is improved when including $3N$ potentials. The curves obtained with the CD-Bonn *NN* potential [4] including (dashed line) and not including (solid line) the Tucson-Melbourne $3N$ potential TM99 [9] are shown in Fig. 2. Predictions obtained with the Argonne AV18 *NN* potential [2] and the Nijmegen potentials Nijm1 and Nijm2 [5], which can also be combined with the TM99 $3N$ potential, are not shown in

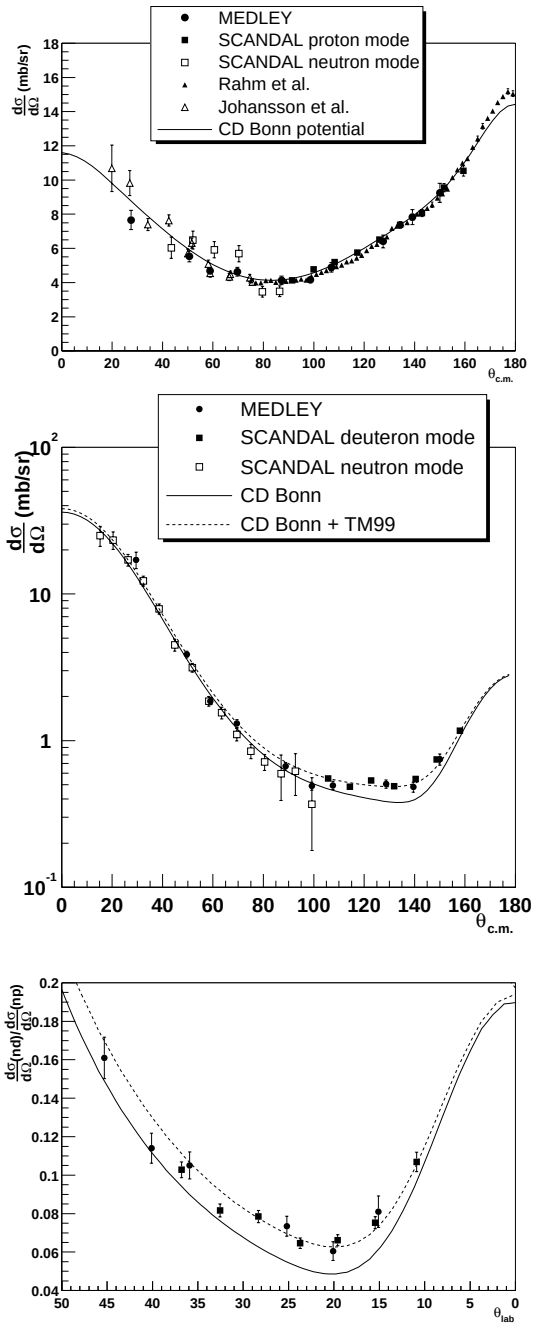


Figure 2: Combined data of the three present experiments, for the *np* (top panel), *nd* (middle panel) and the ratio between *nd* and *np* (bottom panel) elastic scattering differential cross sections at 95 MeV. The theoretical curves for *nd* scattering were obtained with Faddeev calculations [19] with the CD-Bonn (2001) potential [4] without $3N$ forces (solid line) and with the TM99 $3N$ potential [9] (dashed line).

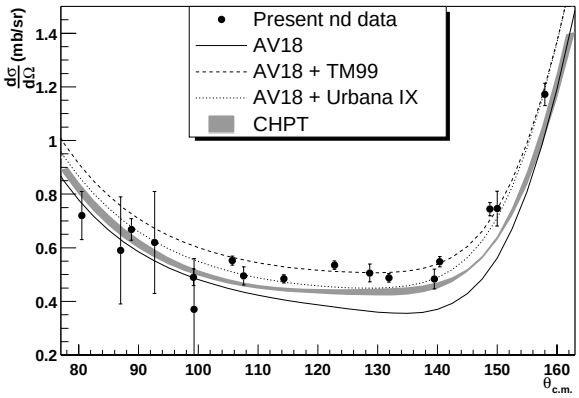


Figure 3: The present *nd* data (filled dots) in the angular range 80°< $\theta_{c.m.}$ <160°. The solid, dashed, and dotted curves were obtained from Faddeev calculations with the Argonne AV18 potential [2] without $3N$ forces, with the Tucson-Melbourne (TM99) $3N$ potential [9], and with the Urbana IX $3N$ potential [11], respectively. The gray band was obtained from chiral perturbation theory at next-to-next-to-leading order [15].

this figure since they give very similar predictions. In the minimum region, our data are well described by the Faddeev calculations including the TM99 $3N$ potential, while they are incompatible with the same calculations without $3N$ forces. This behavior is also observed when considering the ratio of the *nd* to the *np* cross sections (bottom panel of Fig. 2), which is free from normalization uncertainties. The AV18 potential can also be combined with the Urbana IX $3N$ potential [11]. The curve obtained with this choice for the $3N$ force (shown as a dotted line in Fig. 3) gives a different description than the curve obtained with the TM99 $3N$ potential (dashed line). The theoretical prediction obtained from CHPT at next-to-next-to-leading order [15] is shown as a gray band in Fig. 3.

It is quantitatively illustrative to compute the reduced $\chi^2$ between our data and the calculations for the *nd* differential cross section in the minimum, i.e., in the angular range 80°< $\theta_{c.m.}$ <160° (the 17 data points shown in Fig. 3). The reduced $\chi^2$ for different choices of the potentials used in the Faddeev calculations are listed in Table 1. When no $3N$ forces are included, the $\chi^2$ are unreasonably large, in minimum 18. The best description is given by the CD-Bonn potential (version 1996) with the TM99 $3N$ force, with a $\chi^2$ of 2.1. With the AV18 potential, the *nd* differential cross section is slightly better described with the TM99 $3N$ potential ($\chi^2 = 2.3$) than with

Table 1: Reduced $\chi^2$ between the present measured *nd* differential cross section in the minimum (80°< $\theta_{c.m.}$ <160°, or all points shown in Fig. 3) and the Faddeev calculations with different models for the potentials, either without $3N$ forces or combined with a $3N$ potential.

| *NN* potential | Without $3N$ | TM99 [9] | Urbana IX [11] |
|---|---|---|---|
| AV18 [2] | 25 | 2.3 | 3.5 |
| CD Bonn (1996) [3] | 21 | 2.1 | – |
| CD Bonn (2001) [4] | 18 | 2.2 | – |
| Nijm1 [5] | 21 | 3.2 | – |
| Nijm2 [5] | 25 | 2.4 | – |

Table 2: Reduced $\chi^2$ for the ratio of the *nd* to the *np* differential cross sections in the minimum (10°< $\theta_{lab}$ <46°, or all points shown in the bottom panel of Fig. 2). The present data are compared with calculations with different models for the potentials (for *nd* scattering, either without $3N$ forces or combined with a $3N$ potential).

| *NN* potential | Without $3N$ | TM99 [9] | Urbana IX [11] |
|---|---|---|---|
| AV18 [2] | 17 | 2.7 | 1.2 |
| CD Bonn (1996) [3] | 13 | 0.6 | – |
| CD Bonn (2001) [4] | 12 | 1.7 | – |
| Nijm1 [5] | 15 | 3.8 | – |
| Nijm2 [5] | 18 | 2.8 | – |

the Urbana IX potential ($\chi^2 = 3.5$). The CHPT prediction at next-to-next-to-leading order gives a $\chi^2$ of 6.5 (not given in the table). Note that the deviations from unity may be partly due to the normalization uncertainties in the data [46]. For this reason, the ratio of the *nd* differential cross section to the *np* differential cross section− in this ratio, many sources of uncertainties (including the uncertainty in the absolute normalization) are cancelled out−is a more practical observable for testing the models. The reduced $\chi^2$ between our data (for the 13 data points shown in the bottom panel of Fig. 2) and calculations using different *NN* and $3N$ potentials for *nd* scattering are listed in Table 2. When the ratio is considered, the AV18 potential combined with Urbana IX gives a near-perfect description ($\chi^2 = 1.2$), and the best description is still given by CD-Bonn (1996) + TM99 ($\chi^2 = 0.6$).

The present *nd* data can be compared with *pd* data at the same energy to examine the effects of the Coulomb force in *pd* scattering (see Fig. 4).

At 250 MeV, precise *nd* and *pd* data have been published, allowing a detailed analysis of Coulomb effects [62]. The data deviate significantly from

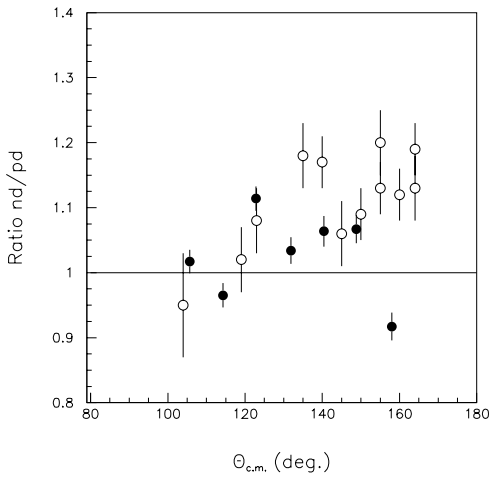


Figure 4: The ratio of *nd* and *pd* scattering cross sections at 95 MeV (filled symbols).The error bars display the full uncertainty, statistical and systematical, with respect to the *nd* data. An additional 5 % uncertainty should be attributed to the *pd* data. The *pd* data have been measured at 90 MeV, and have been scaled down by 8 % to take the energy dependence of the *pd* cross section into account. The unfilled symbols show the same ratio at 250 MeV [62].

the theory predictions. Overall, the ratio is close to unity, but there is an oscillatory behaviour, with *nd* cross sections about 20 % lower than *pd* around 90 degrees, and 20 % higher than *pd* around 120–160 degrees. If this is not due to experimental artifacts, one possible explanation could be isospin dependence in the $2N$ or $3N$ models, or both.

In Fig. 4, the ratio *nd*/*pd* data at 95 MeV is displayed. There is no high-quality *pd* experiment at 95 MeV, but recently data at 90 MeV have been published [63], and an experiment at 100 MeV is under analysis [64]. In the figure, the 90 MeV data have been used, scaled to 95 MeV (8 % reduction in cross section, derived from the energy dependence of predictions based on the AV18 2N force [2] in combination with the U-IX 3N force [11]). No theory prediction of the Coulomb correction is presently available at this energy.

It can be noted that like at 250 MeV, the *nd* data are above the *pd* data

at 95 MeV in the 100-160 degree range, although slightly less so. It should be noted, however, that, if the *pd* data are renormalized further down by 5 %, which is their reported systematic uncertainty, the effect is compatible with the situation at 250 MeV.

# 4 Conclusions

We have measured the full *nd* angular distribution at 95 MeV in three independent experiments, using the MEDLEY setup and the SCANDAL setup either in deuteron or neutron detection mode. The absolute normalization was obtained relative to either the *np* cross section or the total $^{12}$C(n,n) elastic scattering cross section, with an accuracy of $\pm 4\%$. We obtained excellent precision in the angular range of the *nd* cross-section minimum. The data are in good agreement with Faddeev calculations using modern *NN* potentials and including $3N$ forces from a $2\pi$-exchange model, while the calculations without $3N$ forces fail to describe the data. CHPT calculations at next-to-next-to-leading order represent an improvement compared to calculations with *NN* forces only, but still underestimate the data in the minimum region.

The present experimental work provides valuable pieces of information with the purpose of being able to describe nuclear interaction from the basic interactions between nucleons. The *np* and *nd* data help to refine the *NN* and $3N$ potentials as well as effective field theories, which can be applied in systems of more than three nucleons. Thanks to the ongoing advances in computational resources, microscopic calculations directly producing nuclear shell structure from two- and three-nucleon potentials have become feasible and have been attempted for nuclear masses up to A=13 [11, 65]. The inclusion of a $3N$ potential in these calculations has generally a positive effect on the nuclear binding energy and on the level ordering and level spacing of the low-lying excitation spectra. The success of this method depends on the quality of the $3N$ potentials, which can be effectively tested versus experimental data in three-nucleon systems.

# Acknowledgments

We wish to thank the technical staff of the The Svedberg Laboratory for enthusiastic and skillful assistance. We are very grateful to E. Epelbaum, W. Glöckle, H. Kamada and H. Witała for contributions concerning the theoretical part. We have appreciated the precious collaboration of K. Hatanaka and N. Kalantar-Nayestanaki. This work was supported by the Swedish Nuclear

Fuel and Waste Management Company, the Swedish Nuclear Power Inspectorate, Ringhals AB, the Swedish Defence Research Agency and the Swedish Research Council.

# 5 References

## References

[1] M. Lacombe, B. Loiseau, J.M. Richard, R. Vinh Mau, J. Côté, P. Pirès, and R. de Tourreil, Phys. Rev. C **21**, 861 (1980).

[2] R.B. Wiringa, V.G.J. Stoks, and R. Schiavilla, Phys. Rev. C **51**, 38 (1995).

[3] R. Machleidt, F. Sammarruca, and Y. Song, Phys. Rev. C **53**, R1483 (1996).

[4] R. Machleidt, Phys. Rev. C **63**, 024001 (2001).

[5] V.G.J. Stoks, R.A.M. Klomp, C.P.F. Terheggen, and J.J. de Swart, Phys. Rev. C **49**, 2950 (1994).

[6] R. Machleidt and I. Slaus, J. Phys. G **27**, R69 (2001).

[7] W. Glöckle, H. Witała, D. Hüber, H. Kamada, and J. Golak, Phys. Rep. **274**, 107 (1996).

[8] S.A. Coon, M.D. Scadron, P.C. McNamee, B.R. Barrett, D.W.E. Blatt, and B.H.J. McKellar, Nucl. Phys. **A317**, 242 (1979); S.A. Coon and W. Glöckle, Phys. Rev. C **23**, 1790 (1981).

[9] J.L. Friar, D. Hüber and U. van Kolck, Phys. Rev. C **59**, 53 (1999); S.A. Coon and H.K. Han, Few-Body Syst. **30**, 131 (2001).

[10] J. Carlson, V.R. Pandharipande, and R.B. Wiringa, Nucl. Phys. **A401**, 59 (1983).

[11] B.S. Pudliner, V.R. Pandharipande, J. Carlson, Steven C. Pieper, and R.B. Wiringa, Phys. Rev. C **56**, 1720 (1997).

[12] A. Nogga, A. Kievsky, H. Kamada, W. Glöckle, L.E. Marcucci, S. Rosati, and M. Viviani, Phys. Rev. C **67**, 034004 (2003).

[13] A. Nogga, H. Kamada, W. Glöckle, and B.R. Barrett, Phys. Rev. C **65**, 054003 (2002).

[14] Ulf-G. Meissner, Nucl. Phys. **A737**, 110 (2004).

[15] E. Epelbaum, A. Nogga, W. Glöckle, H. Kamada, Ulf-G. Meissner, and H. Witała, Phys. Rev. C **66**, 064001 (2002).

[16] P.F. Bedaque and U. van Kolck, Annu. Rev. of Nucl. Part. Sci. **52**, 339 (2002).

[17] D.R. Entem and R. Machleidt, Phys. Rev. C **68**, 041001(R) (2003).

[18] E. Epelbaum, W. Glöckle, and Ulf-G. Meissner, Nucl Phys. **A747**, 362 (2005).

[19] H. Witała, W. Glöckle, D. Hüber, J. Golak, and H. Kamada, Phys. Rev. Lett. **81**, 1183 (1998).

[20] S. Nemoto, K. Chmielewski, S. Oryu, and P.U. Sauer, Phys. Rev. C **58**, 2599 (1998).

[21] L.D. Knutson, Phys. Rev. Lett. **73**, 3062 (1994).

[22] J. Kuroś-Żołnierczuk, H. Witała, J. Golak, H. Kamada, A. Nogga, R. Skibiński, and W. Glöckle, Phys. Rev. C **66**, 024003 (2002).

[23] O. Chamberlain and M.O. Stern, Phys. Rev. **94**, 666 (1954).

[24] H. Postma and R. Wilson, Phys. Rev. **121**, 1229 (1961).

[25] K. Kuroda, A. Michalowicz, and M. Poulet, Nucl. Phys. **88**, 33 (1966).

[26] G. Igo, J.C. Fong, S.L. Verbeck, M. Goitein, D.L. Hendrie, J.C. Carroll, B. McDonald, A. Stetz, and M.C. Makino, Nucl. Phys. **A195**, 33 (1972).

[27] R.E. Adelberger and C.N. Brown, Phys. Rev. D **5**, 2139 (1972).

[28] H. Shimizu, K. Imai, N. Tamura, K. Nisimura, K. Hatanaka, T. Saito, Y. Koike and Y. Taniguchi, Nucl. Phys. **A382**, 242 (1982).

[29] H. Sakai *et al.*, Phys. Rev. Lett. **84**, 5288 (2000).

[30] R.V. Cadman *et al.*, Phys. Rev. Lett. **86**, 967 (2001).

[31] K. Ermisch *et al.*, Phys. Rev. Lett. **86**, 5862 (2001).

[32] K. Sekiguchi *et al.*, Phys. Rev. C **65**, 034003 (2002).

[33] K. Hatanaka *et al.*, Phys. Rev. C **66**, 044002 (2002).

[34] K. Ermisch *et al.*, Phys. Rev. C **68**, 051001(R) (2003).

[35] K. Sekiguchi *et al.*, Phys. Rev. C **70**, 014001 (2004).

[36] M. Allet *et al.*, Phys. Rev. C **50**, 602 (1994).

[37] M. Allet *et al.*, Phys. Lett. B **376**, 255 (1996).

[38] J. Zejma *et al.*, Phys. Rev. C **55**, 42 (1997).

[39] K. Bodek *et al.*, Few Body Syst. **30**, 65 (2001).

[40] St. Kistryn *et al.*, Phys. Rev. C **68**, 054004 (2003); St. Kistryn *et al.*, Phys. Rev. C **72**, 044006 (2005).

[41] L. Canton and W. Schadow, Phys. Rev. C **62**, 044005 (2000); L. Canton and W. Schadow, Phys. Rev. C **64**, 031001(R) (2001).

[42] A. Kievsky, M. Viviani, and L.E. Marcucci, Phys. Rev. C **69**, 014002 (2004).

[43] A. Deltuva, A.C. Fonseca, and P.U. Sauer, Phys. Rev. C **71**, 054005 (2005).

[44] H. Rühl *et al.*, Nucl. Phys. **A524**, 377 (1991).

[45] P. Mermod *et al.*, Phys. Lett. B **597**, 243 (2004).

[46] P. Mermod *et al.*, Phys. Rev. C **72**, 061002(R) (2005).

[47] P. Mermod *et al.*, Phys. Rev. C **74**, 054002 (2006).

[48] J.N. Palmieri, Nucl. Phys. **A188**, 72 (1972).

[49] Y. Maeda, Ph.D. thesis, University of Tokyo (2004), unpublished.

[50] H. Witała, J. Golak, W. Glöckle, and H. Kamada, Phys. Rev. C **71**, 054001 (2005).

[51] K. Sekiguchi *et al.*, Phys. Rev. Lett. **95**, 162301 (2005).

[52] J. Rahm *et al.*, Phys. Rev. C **63**, 044001 (2001).

[53] C. Johansson *et al.*, Phys. Rev. C **71**, 024002 (2005).

[54] J. Blomgren, N. Olsson, and J. Rahm, Phys. Scr. **T87**, 33 (2000).

[55] M. Sarsour *et al.*, Phys. Rev. Lett. **94**, 082303 (2005).

[56] J. Klug *et al.*, Phys. Rev. C **68**, 064605 (2003).

[57] M.B. Chadwick, P.M. DeLuca Jr., and R.C. Haight, Radiat. Prot. Dosim. **70**, 1 (1997).

[58] J. Blomgren and N. Olsson, Radiat. Prot. Dosim. **103**, 293 (2003).

[59] S. Dangtip *et al.*, Nucl. Instr. Meth. **A 452**, 484 (2000).

[60] J. Klug *et al.*, Nucl. Instr. Meth. **A 489**, 282 (2002).

[61] A.N. Smirnov, V.P. Eismont, and A.V. Prokofiev, Rad. Meas. **25**, 151 (1995).

[62] Y. Maeda, *et al.*, Phys. Rev. C **76**, 014004 (2007).

[63] H.R. Amir-Ahmadi *et al.*, Phys. Rev. C **75**, 041001(R) (2007).

[64] K. Hatanaka, private communication.

[65] P. Navrátil and W.E. Ormand, Phys. Rev. C **68**, 034305 (2003).

# Author Index

# Subject Index